JACS
JOURNAL OF THE AMERICAN CHEMICAL SOCIETY

ARTICLE

pubs.acs.org/JACS

Doped CeO_2−$LaFeO_3$ Composite Oxide as an Active Anode for Direct Hydrocarbon-Type Solid Oxide Fuel Cells

Tae Ho Shin,[†,§] Shintaro Ida,[†,‡] and Tatsumi Ishihara*[,†,‡,§]

[†]Department of Applied Chemistry, Faculty of Engineering, and [‡]International Institute for Carbon Neutral Energy Research (I[2]CNER), Kyushu University, Motooka 744, Nishi-ku, Fukuoka, Japan

[§]Department of Automotive Science, Graduate School of Integrated Frontier Science, Kyushu University, Fukuoka, Japan

Supporting Information

ABSTRACT: Direct utilization of hydrocarbon and other renewable fuels is one of the most important issues concerning solid oxide fuel cells (SOFCs). Mixed ionic and electronic conductors (MIECs) have been explored as anode materials for direct hydrocarbon-type SOFCs. However, electrical conductivity of the most often reported MIEC oxide electrodes is still not satisfactory. As a result, mixed-conducting oxides with high electrical conductivity and catalytic activity are attracting considerable interest as an alternative anode material for noncoke depositing anodes. In this study, we examine the oxide composite $Ce(Mn,Fe)O_2$−$La(Sr)Fe(Mn)O_3$ for use as an oxide anode in direct hydrocarbon-type SOFCs. High performance was demonstrated for this composite oxide anode in direct hydrocarbon-type SOFCs, showing high maximum power density of approximately 1 W cm^{-2} at 1073 K when propane and butane were used as fuel. The high power density of the cell results from the high electrical conductivity of the composite oxide in hydrocarbon and the high surface activity in relation to direct hydrocarbon oxidation.

INTRODUCTION

Fuel cells have received a great deal of attention because they promise to provide clean, environmentally friendly power generation by directly converting chemical energy into electrical energy.[1] Among the various types of fuel cells, solid oxide fuel cells (SOFCs) have many advantages such as high energy conversion efficiency and high stability. In particular, an attractive advantage of solid oxide fuel cells is fuel flexibility because of high energy conversion efficiencies and the system's simple operation,[2−4] offering the possibility of direct utilization of hydrocarbons and other renewable fuels, namely, biofuels. However, the use of hydrocarbon fuel for current SOFCs has been limited because of several challenging issues, such as low anode reliability, i.e., oxidation tolerance in high humidity conditions and deactivation by carbon coking. In addition, the operating temperature of SOFCs is excessively high (1073−1273 K), and thus all materials used for the cell should be stable at high temperatures. Currently, the most commonly used anode materials are metal oxide composites, primarily Ni-based ones. Ni-based anodes show good electrochemical conductivity and catalytic performance for hydrogen oxidation; however, Ni is easily deactivated by carbon formation when it is directly exposed to hydrocarbons.[5−7] In the most serious circumstance, the cells fracture is a result of deposited coke.[8−10] Consequently, replacing Ni-based anodes with a reliable metal such as Cu-based metals or ceramic anodes has recently attracted a great deal of attention.

Oxide anodes have also been investigated as an alternative to overcome the problems associated with Ni anodes. Tao et al. reported that reasonably high power densities could be achieved in $La_{0.75}Sr_{0.25}Cr_{0.5}Mn_{0.5}O_3$ perovskite oxide. Gorte et al. reported that ceria-based ceramic anodes with small amounts of metal additives such as Cu or Pd perform reliably with hydrocarbon fuels. Furthermore, several groups have reported that $SrTiO_3$-based oxides can be used reliably as SOFC anodes.[11−15] The advantages of these oxide anodes are their tolerance to reoxidation and small carbon deposition in hydrocarbon fuels. However, despite some positive results reported for oxide anodes, the power density of the cells at intermediate temperatures is still much smaller than that using a Ni cermet anode because of insufficient electrical conductivity as well as surface activity. Thus far, carbon-tolerant ceramic anodes are mainly studied for use with methane fuel; however, it is still difficult to use higher hydrocarbons such as propane, which are more subject to coke formation compared with CH_4. For the purposes of this study, we have chosen oxide composites as an oxide anode for SOFCs to enhance both catalytic activity and electrical conductivity.[16−19] Mn- and Fe-based perovskite and doped ceria could be used as a catalyst in redox reactions such as electrochemical oxidation of a hydrocarbon, such as propane, although the catalytic properties are strongly dependent on the composition of perovskite.[20,21] In previous research on mixed ionic and electronic conductors (MIEC), we reported on the anodic performance of $La(Sr)MO_3$ (M = Cr, Mn, Fe, Co, Ti, Ni) perovskite oxide and found that Mn-based perovskite shows

Received: July 6, 2011
Published: October 19, 2011

reasonably high anode reaction performance, although the conductivity decreases under low P_{O2} atmospheres such as H_2. In addition, we showed that a relatively good power-generation property as well as excellent redox tolerance was achieved using an oxide composite anode of $Ce_{0.6}Mn_{0.3}Fe_{0.1}O_2$−$La_{0.6}Sr_{0.4}Fe_{0.9}Mn_{0.1}O_3$, denoted as CMF-LSFM. However, the observed power density of the cell using CMF-LSFM is still smaller than that of the cell using Ni-SDC (Sm doped CeO_2) conventional anode.

Furthermore, not only methane but also liquid petroleum gas has various benefits as a suitable fuel for portable SOFC power-generating systems and auxiliary power units for vehicles. Thus, in this study, we examined the applicability of various hydrocarbon fuels for SOFCs using CMF-LSFM composite oxide anodes. Because simple benefit of plant (BOP) was expected, we used a dry condition for the hydrocarbons, which is an extremely difficult condition for coke deposition. We report dramatically improved power densities for the cell using an oxide composite anode under hydrocarbon fuel conditions.

EXPERIMENTAL SECTION

Composite Oxide Anode and Cathode. Oxides of $Ce_{0.6}Mn_{0.3}Fe_{0.1}O_2$ and $La_{0.6}Sr_{0.4}Fe_{0.9}Mn_{0.1}O_3$ were prepared using the conventional solid-state reaction method. The powder was calcined at 1473 K for 6 h in air. The starting reagents used in this study were $Ce(NO_3)_3\cdot 6H_2O$ (98%, Kishinda Chemical Co. Ltd., Japan), $La(NO_3)_3\cdot 6H_2O$ (99.9% Wako Chemical Co. Ltd., Japan), $Sr(NO_3)_2$ (98% Wako Chemical Co. Ltd., Japan), $Fe(NO_3)_3\cdot 9H_2O$ (99% Kishinda Chemical Co. Ltd., Japan), and $Mn(NO_3)_2\cdot 6H_2O$ (99.9% Wako Chemical Co. Ltd., Ltd., Japan). The powders were mixed in an alumina mortar resulting in a composite oxide anode consisting of 12.5 wt % Ce(Mn,Fe)O_2 and La(Sr)Fe(Mn)O_3. Perovskite oxide of $Sm_{0.5}Sr_{0.5}CoO_3$ prepared by the solid-state reaction method was used as the cathode.

Electrolyte Support and Fabrication of the Single Cell. $La_{0.8}Sr_{0.2}Ga_{0.8}Mg_{0.15}Co_{0.05}O_3$ (LSGMC) was used for the electrolyte.[22] We prepared the self-supporting LSGMC electrolyte disk, with a fixed thickness (ca. <0.3 mm), by the tape-casting method and performed the final sintering at 1773 K for 6 h in air. Each face of the LSGMC electrolyte disk having a 5-mm diameter anode and cathode was coated with the obtained electrode powder and then calcined at 1273 K for 30 min. A platinum electrode prepared using commercial Pt paste (Tanaka TR7902) was used as the reference electrode and was placed close to the cathode. We connected the platinum or gold lead wire to the Pt reference electrode.

Measuring Electrical Conductivity of CMF-LSFM Bulk Specimen. To measure electrical conductivity, the powder was first pressed into a rectangular shape, sintered at 1523 K, and then cut to precisely 3 × 3 × 15 mm. We generally used the Pt electrode and measured electrical conductivity by the DC four-probe method.

Cell Testing and Evaluating Electrical Properties. The power-generating properties of SOFCs were measured with four Pt or Au lead lines and Pt or Au mesh (80 mesh) as the current collector in humidified H_2, and dry hydrocarbons and O_2 were used as the fuels and oxidant, respectively. We estimated the IR loss and overpotential of the anode by using the current interruption method. To compare the effects on catalytic performance when using Pt as a current collector with that obtained using Au, the cell performance was also measured with Au lead lines and Au mesh (80 mesh).

Characterization of CMF-LSFM. The obtained crystalline phase stability before and after the cell test was identified using XRD (Rigaku, RINT2500, Cu Kα radiation). Thermal expansion coefficients (TEC) of CMF, LSFM, CMF-LSFM composite, and LSGMC, which were pressed into a rectangular shape and sintered at 1523−1773 K, were measured using a thermomechanical analyzer (TMA, Rigaku type 8310) in air

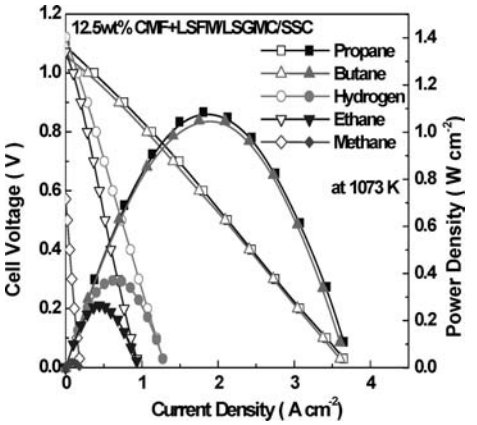

Figure 1. Cell voltage and power density versus current density for a fuel cell with a Ce(Mn,Fe)O_2−La(Sr)Fe(Mn)O_3 composite anode. The electrolyte-supporting cell had an electrolyte thickness <300 μm and $Sm_{0.5}Sr_{0.5}CoO_3$ cathode at 1073 K in hydrogen (●), methane (♦), ethane (▼), propane (■), and n-butane (▲).

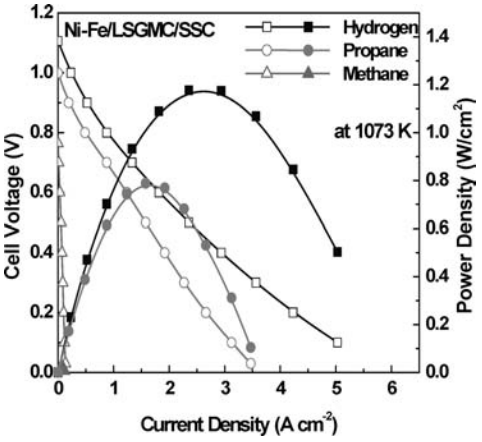

Figure 2. Cell voltage and power density versus current density for a fuel cell with Ni−Fe anode. The electrolyte-supporting cell had an electrolyte thickness <300 μm and $Sm_{0.5}Sr_{0.5}CoO_3$ cathode at 1073 K in hydrogen (■), methane (▲), and propane (●).

from 300 to 1273 K with a heating rate of 5 K min^{-1}. To analyze the carbon coke on the anode material under high carbon atmospheres, the adsorption rate of carbon with 10 vol% C_3H_8 was also measured using an IR spectrometer (JASCO-610) with an MCT detector and an in situ diffuse reflection unit. The measurement devices were connected to a gas-circulating and vacuum system. After evacuation at 773 K for 1 h, the background spectra of CMF-LSFM and Ni-SDC cermet without hydrocarbon adsorption were measured. These powders were exposed to C_3H_8 gas (10 kPa) and heated for 40 min at each temperature under gas-circulating conditions, and the IR measurement was performed at an elevated temperature. As Raman spectroscopy is a useful method to analyze coke deposition on oxide materials, we also used a Horiba HR800 to measure the surface of the CMF-LSFM anode after cell tests under hydrocarbon atmospheres.

RESULTS AND DISCUSSION

Power Generation Property of the Cell Using the CMF-LSFM Anode with Dry Hydrocarbon. Figures 1 and 2 show the current−power density (I−P) and current−terminal voltage

(I−V) curves of the cell using the CMF-LSFM composite oxide and Ni−Fe anodes, respectively, when various hydrocarbons, i.e., hydrogen, methane, ethane, propane, and butane, were used as fuel. In the case of H_2, we achieved a fairly good power density for the cell as reported previously;[19] however, it was much lower than that for the cell using Ni−Fe (9:1) bimetal for the anode. On the other hand, in case of the CMF-LSFM oxide anode, the maximum power density increased as the hydrocarbon's carbon number increased. As shown in Figure 1, the CMF-LSFM oxide anode achieved approximately 1 W cm^{-2} at 1073 K when C_3H_8 or C_4H_{10} were used as fuels. In contrast, as shown in Figure 2, with a conventional Ni−Fe anode, power density decreased as the carbon number increased. When C_3H_8 was used as the fuel, power density drastically decreased over the measurement period, suggesting the deactivation of the anode by coke deposition. The observation that power density increased relative to higher fuel carbon numbers in the cell using the CMF-LSFM oxide anode is very interesting. It is also noted that this power density was extremely large compared to the results reported for ceramic or even metal anodes; the power density of the oxide anode is always smaller than 0.5 W cm^{-2} at 1073 K for hydrogen or methane. Therefore, the cell using the CMF-LSFM composite anode showed unique behavior. This suggests that CMF-LSFM dual oxide composite exhibits superior catalytic activity for complete (eq 1) and partial oxidation (eq 2) of C_3H_8 and C_4H_{10}.

$$C_nH_{2n+2} + (3n + 1)O^{2-} \rightarrow nCO_2 + (n + 1)H_2O + (6n + 2)e^- \quad (1)$$

$$C_nH_{2n+2} + (2n + 1)O^{2-} \rightarrow nCO + (n + 1)H_2O + (4n + 2)e^- \quad (2)$$

Here it is noted that formation of H_2, CO, and small amount of CO_2 was observed in an exhaust gas line with gas chromatographs. Therefore, it seems that partial oxidation reaction was dominant in overall reaction. However, the re-forming reaction of hydrocarbon with formed CO_2 and H_2O successively proceeds because of a small fuel usage in this study (ca. 10%). In addition, quantitative analysis of water is highly difficult, and so, detailed discussion on which reaction is dominant in the present system is difficult at present. However, it seems that both reactions 1 and 2 appear to proceed simultaneously in this study.

In this study, although extremely high power density was observed for the cell using dry C_3H_8 or C_4H_{10} fuel, as shown in Figure 1, it is possible that the Pt current collector used may function as an anode catalyst. Because the experiment was performed with the Pt current collector, a highly active oxidation catalyst, it is still uncertain whether CMF-LSFM dual oxide composite truly exhibits good catalytic activity.[23] It has been reported that, compared to inert current collectors, Pt current collectors have a dramatic effect on the performance of ceramic anodes.[24] On the other hand, the observed power density for other metallic current collectors is almost the same as that of the cell with a Pt current collector in our system, which consisted of the LSGMC electrolyte and the CMF-LSFM composite oxide anode. In addition, as it is well-known that Au displays almost no hydrocarbon oxidation activity, power-generating properties were monitored using Au as the current collector. Figure 3 shows the I−V and I−P curves of the cell using the CMF-LSFM anode and an Au current collector. The cell with an Au current collector shows very similar power density and OCV (open circuit voltage) as the cell using a Pt current collector (Figure1). However, it should be noted that a small decrease in power density was evident because of the insufficient mechanical strength of Au for current collection. Therefore, the effects of the current collector on power density are barely observable, and therefore the effects of Pt mesh can be ignored. In addition, Figure 4 shows the power-generation curves of the cell at 1073 K when Pt mesh was used without an anode layer. Because it has been reported that carbon−Pt is active as an anode in the case of a direct hydrocarbon-type cell,[25] we measured the power-generating property of the cell using only a Pt current collector as the anode. Evidently, almost negligible power density (<10 mW cm^{-2}) is exhibited when a Pt mesh current corrector is used with the LSGMC electrolyte as shown in Figure 4. Although Pt is a well-known anode catalyst, the open circuit potential of the cell (Figure 4) is much smaller than the theoretical potential and the observed power density is much smaller than that of a CMF-LSFM oxide anode. This confirms that the contribution of a Pt current collector on the anode reaction with LSGMC electrolyte is negligibly small in this study. Consequently, the observed high

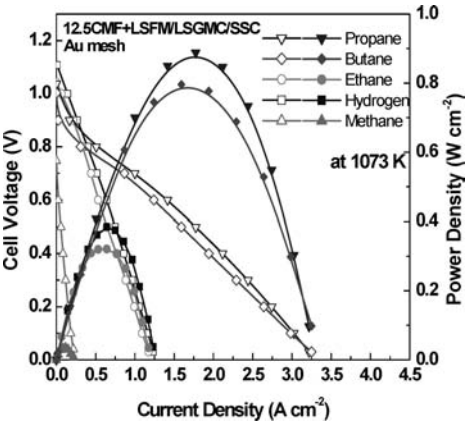

Figure 3. Power-generation curves of a cell using a $Ce(Mn,Fe)O_2$−$La(Sr)Fe(Mn)O_3$ composite anode and Au mesh as a current collector. The electrolyte-supporting cell had an electrolyte thickness <300 μm and $Sm_{0.5}Sr_{0.5}CoO_3$ cathode at 1073 K and hydrogen (■), methane (▲), ethane (●), propane (▼), and n-butane (♦) for fuel.

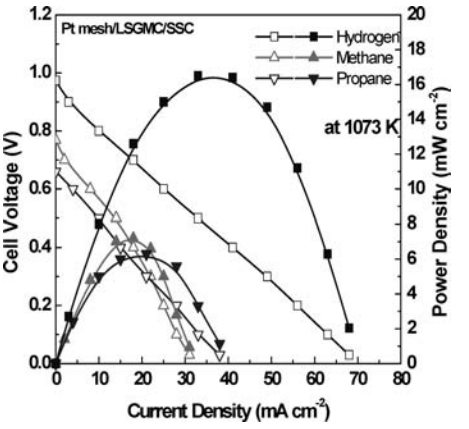

Figure 4. Power-generation curves of a cell using only Pt mesh (80 mesh size) for anode. The electrolyte-supporting cell had an electrolyte thickness <300 μm and $Sm_{0.5}Sr_{0.5}CoO_3$ cathode at 1073 K and hydrogen (■), methane (▲), and propane (▼) for fuel.

dx.doi.org/10.1021/ja206278f |J. Am. Chem. Soc. 2011, 133, 19399–19407

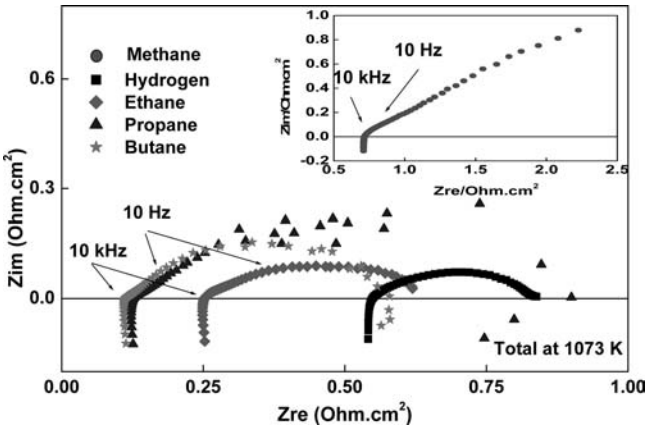

Figure 5. Impedance spectra measured for a cell using $Ce(Mn,Fe)O_2$–$La(Sr)Fe(Mn)O_3$ composite anode at 1073 K in methane (●), hydrogen (■), ethane (♦), propane (▲), and n-butane (★).

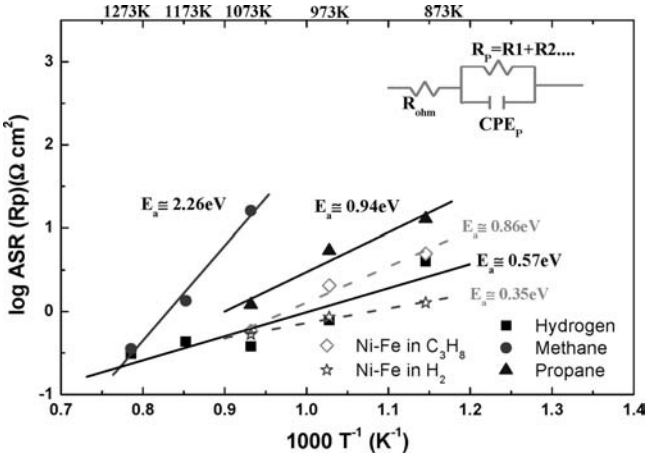

Figure 6. ASR temperature dependence and activation energies for various anodes and fuels. The squares and circles represent the anode ASR values calculated from intermediate and low frequency semicircles in the impedance diagram.

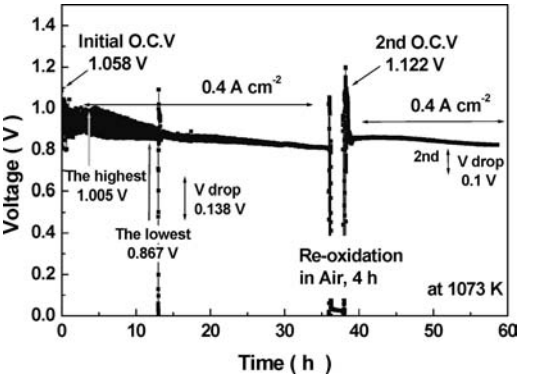

Figure 7. Changes in output voltage of a cell using the $Ce(Mn,Fe)O_2$–$La(Sr)Fe(Mn)O_3$ composite anode at a current density of 0.4 A cm^{-2} operated for 60 h under propane and redox cycles.

power density of the cell using the CMF-LSFM anode without a precious metal catalyst could be attributed to the high surface activity of the composite oxide for C_3H_8 or C_4H_{10} oxidation.

Impedance analysis was conducted to further estimate the internal resistance of the cell. Figure 5 shows the impedance spectra of the cell using the CMF-LSFM anode under open circuit conditions when various dry hydrocarbons were used as fuel. Evidently, the impedance spectrum mainly consists of two semicircles: the ohmic and polarization resistances, which we attributed to the activation and diffusion overpotential. The *x*-axis intercepts at higher frequencies and decreases as the carbon number of hydrocarbons increases, which suggests increased electrical conductivity of the composite oxide anode. This will be discussed in greater detail later in the paper. The size of the anodic impedance semicircles increased slightly as the carbon number increased in the hydrocarbons, with the exception of CH_4. Therefore, the diffusion resistance might be closely related to the molecular weight of the hydrocarbons and molecular bonding in the alkanes. In the case of CH_4, we observed unexpectedly high diffusion resistance. This suggests that the low power density of the cell using CH_4 fuel could be explained by high resistance (IR drop) and high polarization resistance (overpotential). At present, the reason why high diffusion resistance was observed for CH_4 is not clear because the molecular size of CH_4 is much smaller than that of C_3H_8 or C_4H_{10}. The low overpotential may be related to the low activity of CH_4, and surface diffusion to three phase boundary (TPB) regions may be slow because of the low surface coverage of CH_4.

The temperature dependence of the anodic reaction was studied further. Figure 6 shows the area resistance of the anode as a function of temperature and the apparent activation energy of the CMF-LSFM anode and Ni–Fe anode when H_2, CH_4, and C_3H_8 were used directly as fuel. The area-specific resistance (ASR) of the anode was estimated by measuring the impedance spectra under open circuit conditions. At all temperatures, the observed impedance spectra consists of two semicircles: a small one at higher frequency, which could be attributed to activation overpotential, and a large flat semicircle at low frequency, which could be attributed to diffusion resistance. In Figure 6, to compare the surface activity of CMF-LSFM with a conventional anode of Ni–Fe, the temperature dependency of ASR estimated for the semicircle at high frequency is also plotted. Apparently, estimated resistance increases at each temperature on both anode materials for fuels used in the following order: $H_2 < C_3H_8 \ll CH_4$. This suggests that the electrochemical oxidation of CH_4 hardly occurred on either anode material and that of H_2 occurs more easily compared to that of CH_4. This is reasonable considering the chemical activity of these fuels for deep oxidation. The activation energy of the CMF-LSFM anode in propane was 0.95 eV, which is similar to 0.86 eV for the Ni–Fe bimetal anode under the same conditions. The large apparent activation energy (2.26 eV in Figure 6) for the anodic reaction when CH_4 is used as the fuel also suggests limited CH_4 oxidation of CMF-LSFM. In any case, it is also reasonable to assume that the low OCV and power density in CH_4 was due to the low chemical activity of CH_4 and, therefore, to conclude that CH_4 is not a suitable fuel for the cell using the CMF-LSFM anode.

In the case of metal anodes, when dry hydrocarbon was fed, power generation drastically decreased with operation time because of the deactivation of the anode due to coke formation. Therefore, prevention of coke formation poses the most serious challenge for metal anodes currently in use. However, there was no evidence of carbon deposits on the surface of the composite anode in our experiments. Figure 7 shows the long-term stability of a cell using the CMF-LSFM anode with C_3H_8 as the fuel.

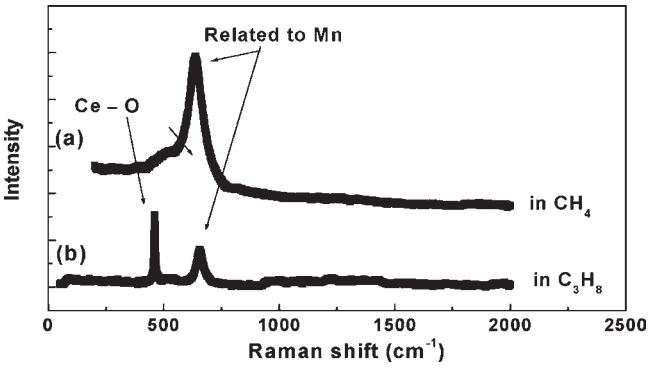

Figure 8. Raman spectra of anodic surface of a cell using the $Ce(Mn,Fe)O_2-La(Sr)Fe(Mn)O_3$ composite anode after long-term operation with propane.

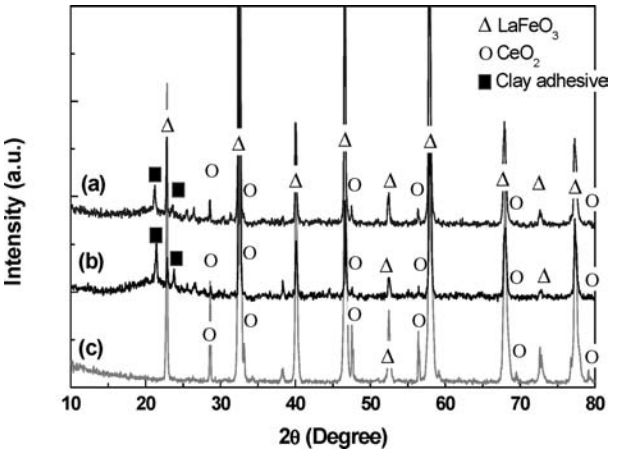

Figure 9. XRD pattern of the surface of the composite oxide anode for a cell using the $Ce(Mn,Fe)O_2-La(Sr)Fe(Mn)O_3$ anode at 1073 K: (c) before as-prepared powder consisting of CMF-LSFM and after cell power-generation measurement; (a) with Pt mesh and (b) Au mesh as a current collector. The peaks marked by black cube indicate the rubber adhesive for holding when the XRD pattern was measured after testing using a small piece of the cell.

As shown in Figure 7, although coke normally forms easily from C_3H_8, degradation by carbon coking was not observed and a stable power-generation property was sustained over 50 h. This suggests that dissociation of the C−H bond in C_3H_8 does not seem to occur on the oxide and that direct oxidation of hydrocarbon mainly occurs on the CMF-LSFM anode. This will be discussed in more detail later in this paper. Thus, CMF-LSFM was highly resistant to coke deposition.

In the initial 10 h, we observed oscillation in the potential that could be related to the repeated redox of the CMF-LSFM anode, in particular, Mn or Fe in oxide. A similar phenomenon is also reported for the Ni anode in H_2 with high P_{H2O}.[26] After 35 h, the oxide anode was exposed to air for 4 h at 1073 K, and then the anode atmosphere was recovered to C_3H_8. After this reoxidation treatment, we observed slightly increased potential. This improvement in OCV and power density is also observed in H_2 fuel,[19] and this seems to be explained by the change in particle size which leads to an improved surface activity and an enlarged contact area, namely the length of the three-phase boundary. After reoxidation treatment, voltage was rapidly and unstably increased and then a few hours, it recovered to almost the same potential as before reoxidation treatment. Oxygen adsorption might remain on the composite oxide, and this adsorption oxygen may lead to a change in electrode reaction, i.e., complete oxidation (eq 1) or partial oxidation (eq 2), resulting in the transient potential change. Detailed analysis of product during the transient period is now under study, and the results will be reported in the future.

To confirm coke deposition, we used Raman spectroscopy to measure the anode after 50 h of operation in CH_4 and C_3H_8 at 1073 K. Figure 8a,b shows the Raman spectra for CH_4 and C_3H_8, respectively. We observed two strong peaks that could be attributed to Ce−O and Mn−O; however, over 50 h of operation, we did not observe peaks between 1350 and 1550 cm^{-1} for either methane or propane. Therefore, no coke deposition occurred on the CMF-LSFM anode after 50 h of operation in C_3H_8. This result corresponds with the stable power-generation property shown in Figure 7 and is consistent with our previous results.[19] Figure 7 also illustrates the effects of the reoxidation treatment of the anode in air at 1073 K. Reoxidation tolerance is another advantage of ceramic anodes and, as demonstrated in our previous study, the power density of the cell did not decrease but in fact increased slightly when exposed to air at operating conditions. Therefore, SOFCs using the CMF-LSFM anode could be highly tolerant of reoxidation, which is also a great advantage of oxide anodes. Furthermore, it could be expected that although coke formation occurred during operation, the cell can be easily recovered by reoxidation treatment. Before the second reoxidation treatment, we introduced H_2 as the fuel and the power density gradually decreased after the fuel was changed. This is consistent with the power-generating property, as shown in Figure 1. After the second reoxidation treatment, the power density recovered to the original level when C_3H_8 was introduced as the fuel again. We also measured the internal resistance of the cell before and after the reoxidation treatment. The internal resistance of the cell barely changed after 50 h of operation in C_3H_8 or after the reoxidation treatment. Therefore, SOFCs using the CMF-LSFM composite oxide for anodes are highly reliable as direct hydrocarbon-type cells, and extremely high and stable power densities (>1 W cm^{-2} at 1073 K) are achieved using C_3H_8 or C_4H_{10}. Because C_3H_8 is actually used for automobile fuel, SOFCs using CMF-LSFM anodes are promising as auxiliary power generators for automobiles.

Figure 9 shows XRD patterns after measuring power generation of the cell using the CMF-LSFM anode. Although the small diffraction peaks from unknown phases were recognized, diffraction peaks mainly consisted of $LaFeO_3$ and CeO_2. This suggests that an oxide phase, a mixture of the partially reduced state of CMF and LSFM, persisted after the power-generating measurement. Obviously, the oxide phase of CMF-LSFM seems to be an active phase for anode reactions. It is known that dissociation of the C−H bond is rather difficult during the oxide phase compared to that of metal, indicating that coke formation may be suppressed on the CMF-LSFM composite oxide.

We studied not only phase stability but also microstructural stability in the CMF-LSFM composite oxide anode during operation with hydrocarbon. Figure 10 shows SEM observation results of the cell using the CMF-LSFM oxide anode after long-term stability measurements in C_3H_8. Evidently, the thickness of both the anode and cathode is uniformly ca. 50 μm. Compared to the cathode, the porosity of anode is slightly greater, and as shown in Figure 10c, the attachment of the anode is high and no

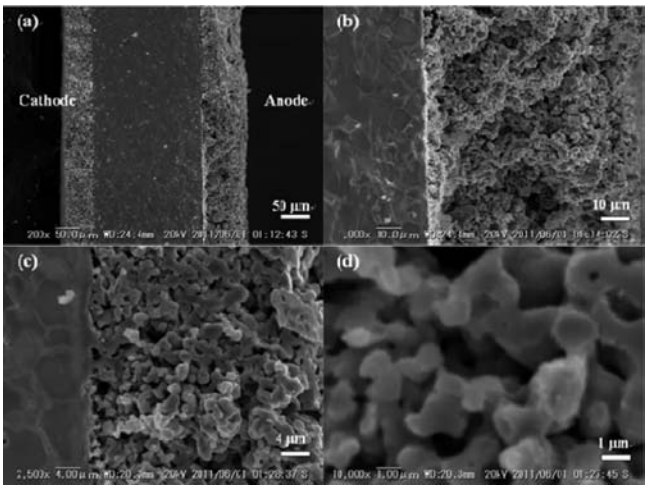

Figure 10. SEM images of a cell using the $Ce(Mn,Fe)O_2$−$La(Sr)Fe(Mn)O_3$ anode after a long-term stability test in C_3H_8 at 1073 K: (a−c) cross-section, and (d) high magnification SEM image of the the CMF-LSFM anode after a long-term test for 50 h in hydrocarbon fuels.

Table 1. Comparison of Internal Resistance in the Cell Using CMF-LSFM as Fuel[a]

fuel	ohmic loss of the anode side ($IR_{a\Omega}$, mV)	anodic overpotential (η_a, mV)	ohmic loss of the cathode side ($IR_{a\Omega}$, mV)	cathodic overpotential (η_c, mV)
H_2	162.49	34.38	9.37	3.12
CH_4[b]	103.13[b]	28.12[b]	12.5[b]	3.13[b]
C_2H_6	40.62	34.38	56.25	3.13
C_3H_8	6.24	3.12	46.87	12.51
C_4H_{10}	6.25	6.25	34.37	21.87

[a] Potential drop at 0.3 A cm^{-2}, cathode; $Sm_{0.5}Sr_{0.5}CoO_3$, electrolyte; $La_{0.8}Sr_{0.2}Ga_{0.8}Mg_{0.15}Co_{0.05}O_3$. [b] Potential drop at 0.2 A cm^{-2}.

delamination is observed even after the reoxidation treatment. In the case of coke deposited from hydrocarbon, it is well-known that filament-like coke was deposited and the catalyst was easily deactivated. However, as shown in Figure 10c,d, there was no evidence of carbon coke deposition, which means there was no filament-like carbon deposition on the anode catalyst. This is in good agreement with the results of the Raman spectroscopy. Therefore, CMF-LSFM is highly active to the anode reaction and also stable with regard to reoxidation and coke deposition.

Electrical Conductivity and Activity of CMF-LSFM Oxide Anode. To understand the high power densities achieved with C_3H_8 and C_4H_{10} fuel, we studied the internal resistance of the cell and the electrical conductivity of the CMF-LSFM composite under operational atmospheres. To better understand the high power densities achieved by C_3H_8 and C_4H_{10} fuel, we hypothesized that electron conduction in CMF-LSFM would be more dominant in the P_{O2} range. Accordingly, we quantified the internal resistance of the cell by measuring the IR loss and electrode overpotential for the cathode and anode during cell operation. Table 1 summarizes the IR loss and electrode overpotential for the cell using the CMF-LSFM anode and various dry hydrocarbons. As shown in Table 1, both the ohmic resistance and the overpotential of the anode side decreased with increasing carbon number during cell operation. The main

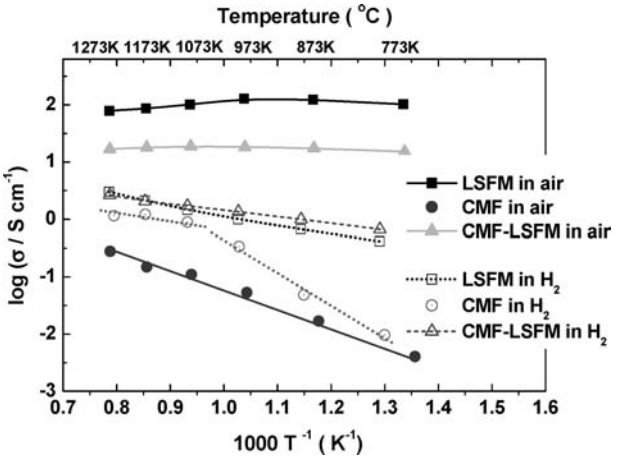

Figure 11. Electrical conductivity of CMF, LSFM, and CMF-LSFM composite oxide in air and H_2 with temperature elevated to 1273 K: electrical conductivity of LSFM in air (■), LSFM in H_2 (□), CMF in air (●), CMF in H_2 (○), CMF-LSFM composite in air (▲) and in H_2 (△).

reason for the potential drop for the current cell is IR loss, in particular on the anodic side. When H_2 was used as fuel, it is evident that the IR loss of the anode is high, and it decreases as the carbon number of the hydrocarbon fuel increases. On the other hand, anodic overpotential also decreased when C_3H_8 or C_4H_{10} was used for fuel. Therefore, internal resistance analysis suggests that the improved power density of C_3H_8 fuel resulted from decreased IR loss and overpotential. Decrease in IR loss is significant and this may be related to the change in the electrical conductivity of the CMF-LSFM composite.

Furthermore, we also examined the change in electrical conductivity in CMF-LSFM using a DC four-probe method with sintered bulk specimens under various controlled atmospheres. Figure 11 shows the temperature dependence of the electrical conductivity of CMF, LSFM and its composite in air, and H_2.

Evidently, in air, LSFM shows much higher electrical conductivity than CMF, and the observed conductivity is close to log $(\sigma/Scm^{-1}) = 2$. However, under a H_2 atmosphere, conductivity decreased drastically to log $(\sigma/Scm^{-1}) = 0$, suggesting that the hole conduction is dominant in LSFM. A-site doped perovskite of the form $La_{1-x}Sr_xFeO_3$ is due to the Sr-induced charge deficiency being balanced by oxygen vacancies and, relative to the neutral lattice, positively charged Fe ions.

Hole conduction in LSFM dominated the total conductivity. In contrast, electrical conductivity of CMF in air is not high as in an electrode; however, it increased when the atmosphere was changed from air to H_2, suggesting that electrical conduction is dominant in CMF. On the other hand, the LSFM and CMF composite in air shows high electrical conductivity, which is attributed to the high conductivity of LSFM. The electrical conductivity decreased when the atmosphere was changed from air to H_2. Therefore, the LSFM-CMF composite is also a p-type semiconductor and hole conduction is dominant in the CMF-LSFM composite in H_2. However, it is interesting that electrical conductivity is slightly higher than that of LSFM in H_2. This suggests that CMF contributes to total conductivity.

Figure 12 shows P_{O2} dependence of electrical conductivity in CMF-LSFM, CMF, and LSFM at 1073 K as a function of oxygen partial pressure. As shown in Figure 12, the total conductivity

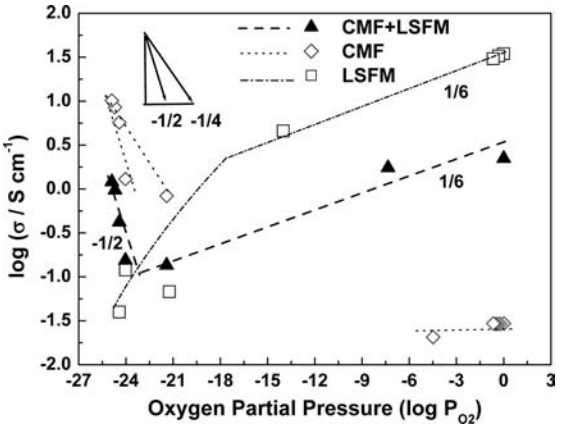

Figure 12. P_{O2} dependence of electrical conductivity in CMF-LSFM (▲), CMF (◇), and LSFM (□) at 1073 K as a function of oxygen partial pressure under various atmospheres controlled by hydrocarbon.

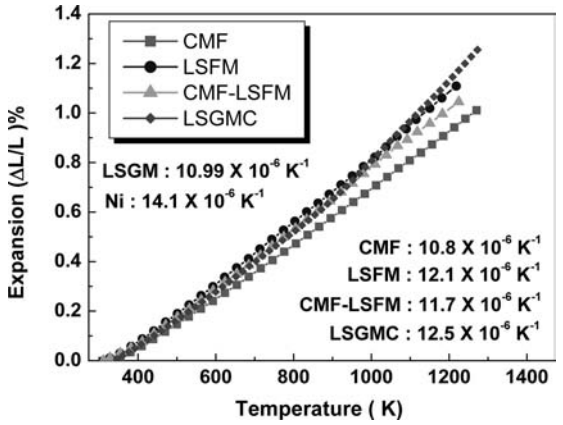

Figure 13. Thermal expansion behavior of CMF-LSFM (▲) composite oxide compared with CMF (■), LSFM (●), and LSGMC (♦). The CTE value of LSGM and Ni is from refs 28 and 29, respectively.

decreased as P_{O2} decreased and reached a minimum level at $P_{O2} = 10^{-20}$ atm. In contrast, electrical conductivity increased as P_{O2} decreased for values lower than 10^{-20} atm, suggesting that p−n transitions occurred at 10^{-20} atm. Hence, n-type semiconductivity was dominant in the low P_{O2} range. With regard to the n-type semiconduction in CeO_2 oxide under reduced atmospheric pressure, the observed increased electrical conductivity could be explained by the partial electronic conduction of Mn- and Fe-doped CeO_2. Furthermore, at low oxygen activity, the electrical conductivity in $La_{1-x}Sr_xFeO_3$ becomes much lower because of p-type semiconduction behavior. Therefore, the decreased IR loss in C_3H_8 and C_4H_{10}, as shown in Table 1, could result from the increased electronic conduction in CMF-LSFM because of n-type semiconduction of CeO_2. Therefore, the improved power densities of the cells using C_3H_8 and C_4H_{10} could be explained by the decreased anodic IR loss, suggesting that the electrical conductivity of the CMF-LSFM composite significantly improved under low P_{O2} atmospheres such as C_3H_8 and C_4H_{10}.

Generally, it is well-known that CeO_2 partially reduces from Ce^{4+} to Ce^{3+} at lower P_{O2}. Due to this reduction, CeO_2 shows partial electronic conductivity, as represented in eq 3:

$$O_2 = V_O^{\bullet\bullet} + 2e' + 1/2\ O_2 \quad (3)$$

Here, $[V_O^{\bullet\bullet}]$ is assumed to be large and so $[e'] \propto {P_{O2}}^{-1/4}$.

Because partial electronic conduction arises from the formed electron, P_{O2} dependence of partial electronic conduction for CeO_2 is reported to be ${P_{O2}}^{-1/4}$ under reduced atmospheric pressure.[27] In fact, as shown in Figure 12, CMF shows P_{O2} dependency of electrical conductivity close to ${P_{O2}}^{-1/4}$ in a range between ca. 10^{-12} to 10^{-21} atm. However, it increased to ${P_{O2}}^{-1/2}$ in the lower P_{O2} range. On the other hand, in the case of CMF-LSFM, the observed P_{O2} dependency of electrical conductivity is only ${P_{O2}}^{-1/2}$. Equation 4, which takes the stable valence number of +3 for Mn and Fe into consideration, represents CMF in reduced atm ($<P_{O2} = 10^{-21}$ atm).

$$M_{Ce}' + O_O^X = (M_{Ce}'' + V_O) + e' + 1/2\ O_2 \quad (M = \text{FeorMn}) \quad (4)$$

In this equation, the valence number of Fe or Mn is changed from +3 to +2 and the formed cation defects are clustered with the formed oxygen vacancy because of the excess amount of oxygen vacancy introduced by formation of reduced state of Fe, Mn, and Ce. Although deposition of metallic Fe or Mn is expected, no metallic state of Fe or Mn was detected by XRD and SEM observation. Therefore, the number of electrons increased as P_{O2} decreased to ${P_{O2}}^{-1/2}$. On the other hand, in the case of high oxygen partial pressure ($>10^{-10}$ atm), electrical conductivity decreases as oxygen partial pressure decreases to ca. ${P_{O2}}^{1/10}$, and in this region, hole conduction in LSFM dominates the total conductivity. Therefore, P_{O2} dependency will be ${P_{O2}}^{1/6}$ in accordance with eq 5.

$$1/2\ O_2 = O_O^X + V_M'' + 2h^{\bullet} \quad (5)$$

Here, M = Fe or Mn in LSFM from electrical neutrality, $2[h^{\bullet}] = [V_M'']$ and so $[h] \propto {P_{O2}}^{1/6}$.

In comparison, as shown in Figure 12, P_{O2} dependency of CMF is almost negligible in the high P_{O2} range, and therefore the overall P_{O2} dependency of the CMF-LSFM becomes smaller than 1/6. In any case, under working conditions for the CMF-LSFM anode with C_3H_8 or C_4H_{10}, electronic conductivity in CMF decreased the overall resistance of the anode resulting in improved power density.

On the other hand, equilibrium oxygen partial pressure, P_{O2}, was calculated with thermodynamic database, "Malt", in various hydrocarbon fuels at 400 mA cm^{-2}, and it is noted that equilibrium oxygen partial pressure decreased with increasing carbon number in fuel (see Table 1, Supporting Information). Therefore, one reason for improved power density could be assigned to the increased electrical conductivity of the composite oxide anode.

One great advantage of an oxide anode is high compatibility in thermal expansion behavior. Therefore, the thermal expansion coefficient was measured. Figure 13 shows the thermal expansion behavior of the CMF-LSFM compared to the LSGMC electrolyte. The CMF-LSFM sample exhibits almost linear thermal expansion from room temperature to 1273 K, and the average coefficient of thermal expansion (CTE) is about $11.7 \times 10^{-6}\ K^{-1}$, while LSGM and Ni has an average CTE of $10.99 \times 10^{-6}\ K^{-1}$ and $14.1 \times 10^{-6}\ K^{-1}$.[28,29] In addition, the thermal expansion behavior of the LSGMC electrolyte in air was examined and the CTE was about $12.5 \times 10^{-6}\ K^{-1}$, as shown in Figure 13. Their similar thermal expansion properties indicate that the CMF-LSFM composite oxide anode has optimal thermal

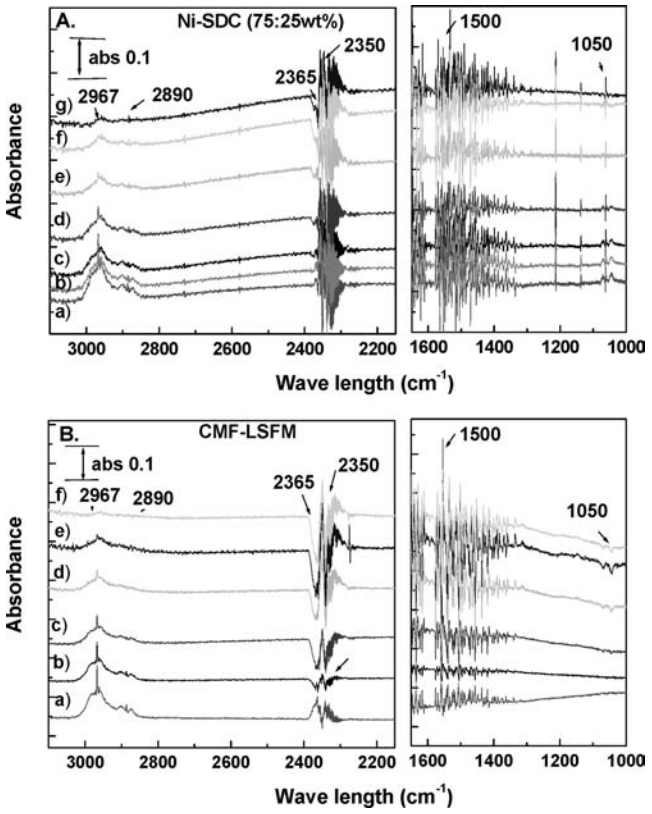

Figure 14. FT-IR patterns of Ni−SDC cermet (A), prepared by reduction of the NiO−SDC composite at 1073 K for 2 h in H_2 at various temperatures for 40 min: (a) adsorption at room temperature; (b) at 373 K; (c) at 473 K; (d) at 573 K; (e) at 673 K; (f) at 773 K; (g) evacuation at 773 K for 1 h. Compared with CMF-LSFM (B) under similar conditions: (a) adsorption at room temperature; (b) at 373 K; (c) at 473 K; (d) at 573 K; (e) at 673 K; (f) evacuation at 673 K for 1 h.

compatibility with the LSGM base electrolyte in the SOFC under normal operational temperatures. Therefore, the SOFCs using a CMF-LSFM anode would be highly resistant to reoxidation and carbon coking, which are both great advantages of oxide anodes.

To confirm the adsorption state of C_3H_8 on an oxide anode, in situ IR spectra of C_3H_8 adsorption were measured on the CMF-LSFM composite powder and the Ni-SDC cermet as a reference sample. Figure 14a,b shows the IR spectra of adsorbed C_3H_8 at elevated temperatures for Ni-SDC and CMF-LSFM, respectively. On both anode materials, IR absorption peaks were observed around 3000, 2300, 1500, and 1050 cm^{-1}, which are attributed to C−H, CO_2, H_2O (or C−H or C−C), and C−O, respectively.[30−32] For Ni-SDC, a decrease in C−H absorption peaks was observed at temperatures higher than 300 °C and around 1050 cm^{-1}, which could be attributed to the decrease of C−O (aldehyde or ketone) at similar temperatures. Therefore, oxidation of C_3H_8 seems to occur on the oxygenated compound on the conventional Ni-SDC anode. It is also noted that, for this experiment, no oxygen exists in gas phase, and therefore oxygen in CeO_2 could be used to form oxygenated compounds. Oxygenated compounds seem to form at around room temperature, and consequently dissociation of C_3H_8 on Ni easily occurs. On the other hand, on the CMF-LSFM composite, at around 3000 cm^{-1}, the IR absorption band decreased at temperatures higher than 473 K and CO_2 peaks strengthened, which suggests that oxidation of C_3H_8 starts at temperatures lower than those for Ni-SDC. This also suggests that CMF-LSFM is highly active to oxidation of C_3H_8. In addition, no peaks were observed at around 1050 cm^{-1} at room temperature. Peaks were only observed at temperatures higher than 673 K. This suggests that oxygenated compounds such as ketone or aldehyde do not form easily because there is no dissociation of the C−C bond. The oxidation of C_3H_8 on CMF-LSFM seems to proceed directly from C_3H_8 but not through an oxygenated compound. This may be effective for preventing coke formation because the polymerization of CH_2 or CH_3 species is precluded. After the gas evacuation phase, absorption peaks around 3000 cm^{-1} were still observed for both catalysts; however, compared to Ni-SDC, the absorbance of C−H peaks was weaker on CMF-LSFM. Therefore, it is reasonable to conclude that the adsorption of C_3H_8 on CMF-LSFM is weaker than that of Ni-SDC. This weak adsorption of C_3H_8 could be attributed to CMF-LSFM's low rate of cleavage of the C−C bonds. CMF-LSFM seems to be highly active with regard to direct C_3H_8 oxidation but not to coke formation.

This study reveals that CMF-LSFM shows n-type semiconductivity under reduced atmospheric pressure and high electrochemical activity for C_3H_8 oxidation. Therefore, this composite oxide is suitable for use as an oxide anode for direct hydrocarbon-type SOFCs.

CONCLUSIONS

The most important consideration thus far for SOFCs is increased reliability as a power generator. For this purpose, development of an oxide anode that resists carbon deposition, reoxidation, and sulfur poisoning is highly desirable. In this study, we have reported improved cell performance with the composite anode for direct hydrocarbon-type SOFCs. The high power densities (>1.0 W cm^{-2}) achieved with C_3H_8 or C_4H_{10} fuel resulted from decreased IR loss and overpotential of the anode. Furthermore, no carbon coke was evident after a long-duration test when C_3H_8 or CH_4 was used as fuel. Low electrical conductivity is always a drawback of oxide anodes,; however, under high oxygen partial pressure, high hole conduction was observed for CMF-LSFM. Moreover, under decreased atmospheric pressure (<10^{-20} atm), conductivity increased as P_{O2} decreased and P_{O2} dependency was ca. −1/2. The observed conductivity is reasonably high, but it is still not sufficiently high for use as an electrode. The TEC of CMF-LSFM also corresponds closely with that of LSGM or LSGMC. The adsorption state was also measured with in situ IR, and it was found that CMF-LSFM shows high activity for direct oxidation of C_3H_8. Therefore, SOFCs using a CMF-LSFM anode are an attractive option for direct hydrocarbon-type SOFCs, and reasonably high power density is achieved when C_3H_8 or C_4H_{10} is used as fuel.

ASSOCIATED CONTENT

Supporting Information. Equilibrium oxygen partial pressure, P_{O2}, was calculated with the thermodynamic database, "Malt", in various hydrocarbon fuels at some current densities. This material is available free of charge via the Internet at http://pubs.acs.org.

AUTHOR INFORMATION

Corresponding Author
ishihara@cstf.kyushu-u.ac.jp

REFERENCES

(1) Service, R. F. *Science* **1999**, *285*, 682.
(2) Minh, N. Q. *Solid State Ionics* **2004**, *174*, 271.
(3) Singhal, S. C. *Solid State Ionics* **2002**, *152*, 405.
(4) Ishihara, T., Ed. Perovskite Oxide for Solid Oxide Fuel Cell. In *Fuel Cells and Hydrogen Energy*; Springer: New York, 2005.
(5) Murry, E. P.; Tasai, T.; Barnett, S. A. *Nature* **1999**, *400*, 649.
(6) Huang, P.; Horky, A.; Petric, A. *J. Am. Ceram. Soc.* **1999**, *82*, 2402.
(7) Steele, B. C. H.; Kelly, I.; Middleton, H.; Rudkin, R. *Solid State Ionics* **1988**, *28*, 1547.
(8) McIntosh, S.; Gorte, R. J. *Chem. Rev.* **2004**, *104*, 4845.
(9) Kim, T.; Liu, G.; Boaro, M.; Lee, S.-I.; Vohs, J. M.; Gorte, R. J.; Al-Madhi, O. H.; Dabbousi, B. O. *J. Power Sources* **2006**, *155*, 231.
(10) Kim, H.; Lu, C.; Worrell, W. L.; Vohs, J. M.; Gorte, R. J. J. *Electrochem. Soc.* **2002**, *149*, A247.
(11) Tao, S.; Irvine, J. T. S.; Kilner, J. A. *Adv. Mater.* **2005**, *17*, 1734.
(12) Kim, G.; Gross, M. D.; Wang, S.; Vohs, J. M.; Gorte, R. J. *J. Electrochem. Soc.* **2008**, *155*, B360.
(13) Lee, S.; Kim, G.; Vohs, J. M.; Gorte, R. J. *J. Electrochem. Soc.* **2008**, *155*, B1179.
(14) McIntosh, S.; Vohs, J. M.; Gorte, R. J. *J. Electrochem. Soc.* **2003**, *150*, A1305.
(15) Tao, S.; Irvine, J. T. S.; Kilner, J. A. *Nat. Mater.* **2003**, *2*, 320.
(16) Ishihara, T.; Shin, T. H.; Vanalabhpatana, P.; Yonemoto, K.; Matsuka, M. *J. Electrochem. Solid State Lett.* **2010**, *13*, B95.
(17) Ishihara, T.; Fukui, S.; Enoki, M.; Matsumoto, H. *J. Electrochem. Soc.* **2006**, *153*, A2085.
(18) Ishihara, T.; Shin, T. H.; Vanalabhpatana, P. *ECS Trans.* **2009**, *25*, 2223.
(19) Shin, T. H.; Vanalabhpatana, P.; Ishihara, T. *J. Electrochem. Soc.* **2010**, *157*, B1896.
(20) Beckers, J.; Drost, R.; Zandvoort, I.; Collignon, P. F.; Rothenberg, G. *Chem. Phys. Chem.* **2008**, *9*, 1062.
(21) Kammer, K.; Skou, E. M. *Solid State Ionics* **2005**, *176*, 915.
(22) Ishihara, T.; Shibayama, T.; Nishiguchi, H.; Takita, Y. *Solid State Ionics* **2000**, *132*, 209.
(23) Gross, M. D.; Vohs, J. M.; Gorte, R. J. *J. Mater. Chem.* **2007**, *17*, 3071.
(24) Kim, G.; Lee, S.; Shin, J. Y.; Corre, G.; Irvine, J. T. S.; Vohs, J. M.; Gorte, R. *J. Electrochem. Solid State Lett.* **2009**, *12*, B48.
(25) McIntosh, S.; Vohs, J. M.; Gorte, R. J. *J. Electrochem. Solid State Lett.* **2003**, *6*, A240.
(26) Murakami, K.; Matsui, T.; Kikuchi, R.; Muroyama, H.; Eguchi, K. *J. Electrochem. Soc.* **2010**, *157*, B880.
(27) Litzelman, S. J.; Tuller, H. L. *Solid State Ionics* **2009**, *180*, 1190.
(28) Ishihara, T.; Honda, M.; Shibayama, T.; Minami, H.; Nishiguchi, H.; Takita, Y. *J. Electrochem. Soc.* **1998**, *145*, 3177–H.
(29) Mori, M; Yamamoto, T; Itoh, H; Inaba, H; Tagawa, H *J. Electrochem. Soc.* **1998**, *145*, 1374.
(30) Zhang, L; Lan, R; Petit, C. T. G; Tao, S. *Int. J. Hydrogen Energy* **2010**, *35*, 6934.
(31) Yi, X. D.; Zhang, X. B.; Weng, W. Z.; Wan, H. L. *J. Mol. Catal. A: Chem.* **2007**, *277*, 202.
(32) Baldia, M.; Finocchiob, E.; Pistarinob, C.; Busca, G. *Appl. Catal., A* **1998**, *173*, 61.